J Fluoresc (2016) 26:821–834
DOI 10.1007/s10895-016-1770-y

ORIGINAL ARTICLE

Effects of Structure and Environment on the Spectroscopic Properties of (3-Amino-*Substituted*-Thieno[2,3-*b*] Pyridine-2-yl) *Pyridine*/*Quinolin*-2-yl)(Phenyl)Methanones: Experimental and Theoretical Study

Ibrahim Ahmed Z. Al-Ansari[1]

Received: 13 November 2015 / Accepted: 14 January 2016 / Published online: 9 February 2016

Abstract The electronic absorption, excitation and fluorescence properties of two 3-amino-*substituted*-thieno[2,3-*b*-]*pyridine*/*quinolin*-2-yl)(phenyl)methanones; (referred to as compounds **1–2:** where 3-amino-4,5,6-trimethyl-thieno[2,3-*b*]*pyridin*-2-yl)(phenyl)methanone (**1**); and 3-amino-5,6,7,8-tetrahydro-thieno[2,3-*b*]*quinolin*-2-yl)(phenyl)methanone (**2**)) have been investigated in solvents of various polarity and hydrogen-bonding abilities. Results based on the electronic absorption, excitation and emission study of these compounds; indicated that singlets (S_1 and S_2) excited-states are populated in non-polar and polar protic/aprotic solvents giving dual fluorescence with weak charge transfer separation. The experimental results were interpreted with the aid of quantum chemistry calculations carried out with the DFT and TD-DFT/B3lyp/6–31 + G(d,p) methods. Based on these calculations, compounds **1–2** exist in two rotamers: *anti* and *syn*, separated by ca. 5–6 kcal mol^{-1} energy barriers in favor of the *anti*-conformer. The *anti*-structure, was shown to be stabilized through existence of intramolecular NH…O hydrogen bond (H-b), which plays a dominant role in affecting the energy of the HOMO-1 molecular orbital. Further, methyl/alkyl substitution in the pyridyl-thiophene ring was shown to involve in σ-π hyper-conjugation and destabilization of the HOMO-1 MO's.

Keywords Absorption · Fluorescence · Intramolecular charge-transfer · Hydrogen bonding · Density functional theory · Time-dependent density functional theory · And solvatochromism

Introduction

Intermolecular and intramolecular interactions are considered a cornerstone in modern research in science, such as chemistry, biology and biophysics. The two most important intermolecular interactions are hydrogen bonding and Vander Waals, due to their key role in DNA, RNA and protein [1–4].

Recent recommended definition of the hydrogen bond states: "*The hydrogen bond is an attractive interaction between a hydrogen atom from a molecule or a molecular fragment X-H in which X is more electronegative than H, and an atom or a group of atoms in the same or different molecule*; *in which there is evidence of bond formation*." [5].

Hydrogen bonding interaction of a solute molecule with solvents like water, alcohols or other amphiprotic solvents can have great impact in terms of solubility, molecular structure and chemical properties of the solute. In this regard, numerous studies exist in the literature that focused on the influence of solvents on the parts of solute's that are sites for hydrogen bonding i.e., $C \equiv N$, $S = O$, $P = O$ and $C = O$ groups [6–9].

The energies of the intermolecular H bonds have been extensively studied in the ground state by different experimental and theoretical methods [10–15]. However, recently, attention has been devoted towards electronic excited-state intermolecular H bonds in carbonyl containing chromophores in order to get a better understanding of hydrogen bonding dynamics in electronically excited states [16–17]. In some novel chromophores, theoretical investigation has shown that competition

Electronic supplementary material The online version of this article (doi:10.1007/s10895-016-1770-y) contains supplementary material, which is available to authorized users.

✉ Ibrahim Ahmed Z. Al-Ansari
iaalansari@qatar.net.qa; iaalansari@gmail.com

[1] Department of Chemistry & Earth Sciences, College of Arts & Sciences, Qatar University, P.O. Box: 2713, Doha, Qatar

between intermolecular- and intramolecular H bonds exist, such as the one in amino-fluorenones [18]. In this study, a conclusion reached was that the internal conversion (IC) process from S_1 to S_0 state is facilitated by intermolecular hydrogen bond strengthening in the excited state.

On the other hand, intramolecular hydrogen bond like intermolecular hydrogen bond has a significant effect on the molecular structure and properties of many chromophores. In this regard, it has been observed that the stability of the intramolecular hydrogen bond formed in many compounds, is due to formation of a six-membered ring; thus giving highly conjugated planar stable structure. This high stability has been named resonance-assisted hydrogen bonding (RAHB) [19]. Recently, using NMR technique, researchers showed that two distinct intramolecular hydrogen bonds in polysubstituted 5-nitropyrimimides with two competing N-H groups exist and influenced by the substituents in these compounds [20].

The hybrid density functional theory (DFT) methods have been widely used to study the strength of the hydrogen bond; which is calculated as the difference between the enthalpies of the structure with and without this bond [21–24]. The B3LYP [25–26] hybrid functional with various basis sets [23, 27–31] has been used for geometry optimization. As far as the basis sets to be used, the inclusion of polarization and diffuse functions is required to obtain reliable results. Moreover, 6–31 + G(d) would be the minimum basis set required to study H bond in large biological systems [32].

In this work, absorption, excitation and fluorescence of two structurally related 3-amino-*4,5,6-trimethyl*-thieno[2,3-*b*-]*pyridine* − 2-yl)(phenyl)methanone (compounds **1**), and 3-amino-*5,6,7,8-tetrahydro*-thieno[2,3-*b*]*quinolin*-2-yl)(phenyl)methanone (compounds **2**), were studied (see Fig. 1). The main focus of this work is elucidation of the role of both intermolecular and intramolecular hydrogen bonding on the ground and excited state dynamics of these chromophores. We have also utilized theoretical calculations of the electronic structures and the optical properties of these molecules to understand the effect of structure and media on the ground and excited-state's solute solvents interactions.

Because DFT predicts structural properties in reasonable agreement with experimental values [21–24], the lowest energies of compounds **1–2** and their complexes with alcohol molecules; were obtained at the DFT B3LYP/6–31 + G(d,p) level of theory using the Gaussian 09 program package [33]. Excitation energies in the gas-phase and different media with various polarities were obtained utilizing time-dependent density functional theory (TD-DFT) [34] with the same functional and basis set.

In the following section we briefly describe the experimental procedure and computational protocol. Illustration and discussion of the results will be given in section 3 and we will give our conclusions in section 4.

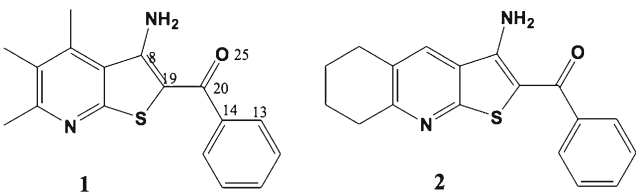

Fig. 1 Structural formula of compounds **1–2**. The atomic numbering used throughout this study is indicated for compound **1** as an example

Experimental

Materials

Compounds **1–2** were purchased from Fluka Co. These compounds were further purified by recrystallization from 90:10 ethanol: water mixture and then vacuum sublimed. Compounds **1** and **2** are yellow solids with m.p. 195–97 °C and 202–203 °C, respectively. The purity of the title compounds **1–2,** was checked with gas chromatography-mass spectrometry. EI-MS, **compound 1** m/z 298 (20) [M + 1], 297 (100) [M + *], 296 (23) 219 (11), and 325 (13); **Compound 2** m/z 310 (21) [M + 1], 309 (100) (M + *], 219 (24), 308 (20), 253 (18), 251 (14), 231 (12).

Solvents

Spectroscopic grade n-hexane, dichloromethane, acetonitrile, ethanol, methanol and butanol were purchased from Fluka chemical Co. and used as received.

Sample Preparation

Stock solutions (1×10^{-4} M) of the compounds were prepared by dissolving the accurate amount of these compounds in *n*-hexane from which 1 mL was withdrawn and added to a 10 mL flask. This was then evaporated by nitrogen bubbling to leave a thin film. The desired solvent was then added and completed to the mark to give final concentrations of 1×10^{-5} M and 1×10^{-5} M for compounds **1–2,** respectively.

Optical Measurements

Spectra recorded with the following spectrometers: Shimatzu UV-160 spectrometer (UV-Vis) and Shimatzu RF-500 spectrometer (fluorescence and exCitation spectra). Emission spectra were obtained using a small angle (90°) front surface excitation geometry. Excitation and emission slits were both 0.5 mm. The experiments were carried out at room temperature (24–25 °C), using 1 cm matched quartz cells. Fresh solutions were used for all measurements emission spectra were not corrected for the spectral response of the instruments.

Quantum Chemical Calculations

Optimized geometries of all structures in the ground-state, were obtained using density functional theory (DFT). Becke's three-parameter hybrid exchange functional (B3) [35] with the Lee-Yang-Parr gradient-corrected (LYP) correlation function [36] was used in conjunction with the 6–31 + G(d,p) basis set [37].

Calculations of harmonic vibrational frequencies and IR intensities to characterize all the stationary points as minima (no imaginary frequencies) were also accomplished at the same level of theory. Excitation energies and oscillator strengths were determined using time-dependent (TD-DFT) calculations [34] at the same functional and basis set. All singlet and triplet configurations from the highest occupied to the 10 lowest unoccupied orbitals were involved in the calculations. The effect of the bulk solvent and specific solute-solvent interaction (for complexes) on the geometry and transition energies was modeled with the conductor-like polarizable continuum model (CPCM) [38], adopted in the linear response formalism when used with TD-DFT. Atomic charges were calculated using the Mulliken population analysis using the same functional and basis set.

Electrostatic potential maps were generated from the calculated electron densities using B3LYP exchange-correlated functional on the ground-state optimized geometries. The maps are colored, identifying regions of high and low electrostatic potentials. All structures were checked by vibrational analysis at B3LYP/6–31 + G(d,p) level of theory and found to be true energy minima. The calculated ν_{NH} and $\nu_{C=O}$ frequencies were visualized with the GausView 5.0.9 package. No corrections were made for the zero point energies, and the force constants were not corrected; since no comparisons were made with experimental vibrational values.

Results and Discussion

Electronic Absorption Spectra

Absorption in non-Polar and Polar Aprotic Solvents

Compounds **1** and **2** give identical absorption spectra in non-polar and polar protic solvents. Figure 2 displays electronic absorption spectra in *n*-hexane. These spectra consist primarily of four distinctive separated bands. The first high-energy band (band **I**) is intense with slight vibronic feasures in the range 200–230 nm. The second absorption band (band **II**) is slightly structured with two peaks in the range 230–300 nm, and its intensity is lowered relative to band **I**. The third band (band **III**) is structured with three distinctive peaks and is found in the region 300–350 nm. The fourth band (band **IV**) appears in the range 350–500 nm domains as one structureless broad peak.

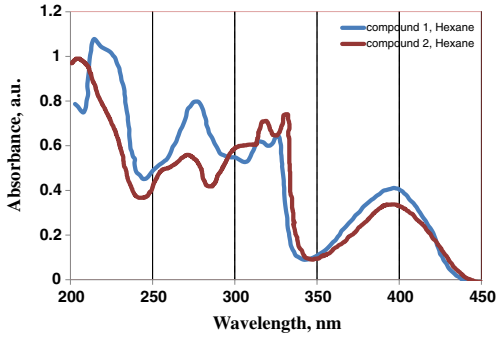

Fig. 2 Absorption spectra of compounds **1–2** in *n*-hexane

Band **III** shows a slight blue shift from a non-polar *n*-hexane to the polar acetonitrile solvents ca. 2 nm and 3 nm, in compounds **1** and **2**, respectively. Band **IV**, on the other hand, is located at 397 and 400 nm (n-hexane) and 389 nm and 403 nm (acetonitrile) for compounds **1** and **2**, respectively. This gives a solvatochromic shift of $\Delta\lambda$ = 7.5 nm and 3 nm for compounds **1** and **2**, respectively. This rather small solvatochromic shift indicates that the product of the ground state dipole moment and the difference between the difference between the ground and excited state dipoles is small [38].

Absorption Spectra in Protic Solvents

Absorption spectra recorded in protic solvents for compounds **1–2** differ from those recorded in aprotic solvents. In protic solvents both compounds **1** and **2**, show all four distinctive bands but with a slight loss of vibrational feasures for band **III**. An example of which is given for ethanol solution in Fig. 3. Moreover, band **III** and **IV** in compounds **1** and **2** show a red shift in the order: methanol < ethanol < butanol (see Table 1 and Fig. 3).

Emission Spectra

Emission Spectra in non-Polar Solvents

Figure 4a-d, shows the fluorescence excitation and emission spectra of compounds **1–2** in non-polar *n*-hexane.

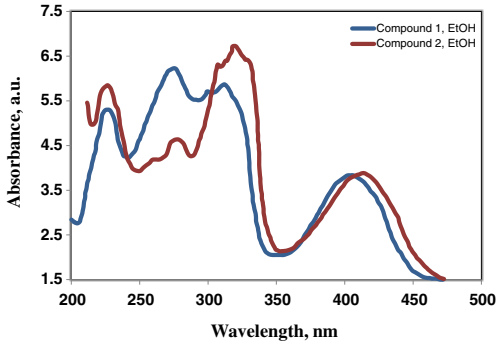

Fig. 3 Absorption spectra of compounds **1–2** in Ethanol

Table 1 Experimental spectroscopic parameters of compounds 1–2 in selected non-polar (aprotic and protic) solvents

	1			2		
	absorption		fluorescence	absorption		fluorescence
	λ_{max} nm [eV[	ε	λ_{max} nm [eV]	λ_{max} nm [eV]	ε	λ_{max} nm [eV]
Hexane	315[3.93] 326[3.80] 389.5[3.18]	1.20 1.23 0.81	364[b][3.40] 475[c][2.61]	317.5[3.90] 331[3.74] 400[3.10]	1.43 1.52 0.70	355[b][3.49] 468[b][2.65] 470[d][2.64]
CH_2Cl_2	318[3.90] 326.5[3.79] 400[3.10]	1.30 1.43 0.87	485[d][2.55]	320.5[3.87] 331.5[3.74] 401[3.09]	1.55 1.71 0.75	365[d][3.39]
ACN	316[3.92] 324[3.83] 397[3.12]	1.8 1.36 0.90	386[b][3.21] 470[d][2.64]	317.5[3.90] 328[3.78] 403[3.07]	1.48 2.56 0.76	365[b][3.39] 480[d][2.58]
MeOH	313[3.96] 322.5[3.80] 403.5[3.10]	1.61 1.45 0.86	480[d][2.58]	317.5[3.90] 326.5[3.79] 409.5[3.03]	1.98 1.80 0.79	365[b][3.39]
EtOH	315[3.93] 322.5[3.80] 406[3.05]	1.50 1.44 0.89	475[d][2.61]	318[3.90] 327.5[3.78] 411.5[3.01]	1.85 1.71 0.78	365[b][3.39] 475[b][2.61] 475[d][2.61]
ButOH	317[3.91] 330[3.76] 408[3.04]	1.70 1.89 1.20	392[b][3.16] 480[b][2.58] 485[d][2.55]	319[3.90] 330[3.78] 414[2.99]	1.16 0.98 0.51	365[b][3.39] 485[b][2.55] 485[d][2.55]
Onset, $E_{0,0}(S_1)$ 446 [2.780 eV]				432.5 [2.866 eV]		
$E_{0,0}(S_2)$ 345 [3.594 eV]				337.5 [3.673 eV]		
ΔE_{gap}[f] 5855.72 cm^{-1} [0.726 eV]				5444.40 cm^{-1} [0.675 eV]		

[a] Molar absorption coefficients have the unit 10^4 x dm^3 mol^{-1} cm^{-1}

[b] λ_{ex} = 326 nm[3.80 eV]

[c] λ_{ex} = 319 nm[3.88 eV]

[d] λ_{ex} = 400 nm[3.10 eV]

[e] Onset taken from excitation emission spectra in cyclohexane

[f] ΔE_{gap} is the energy gap between the S_1 and S_2 states in cyclohexane

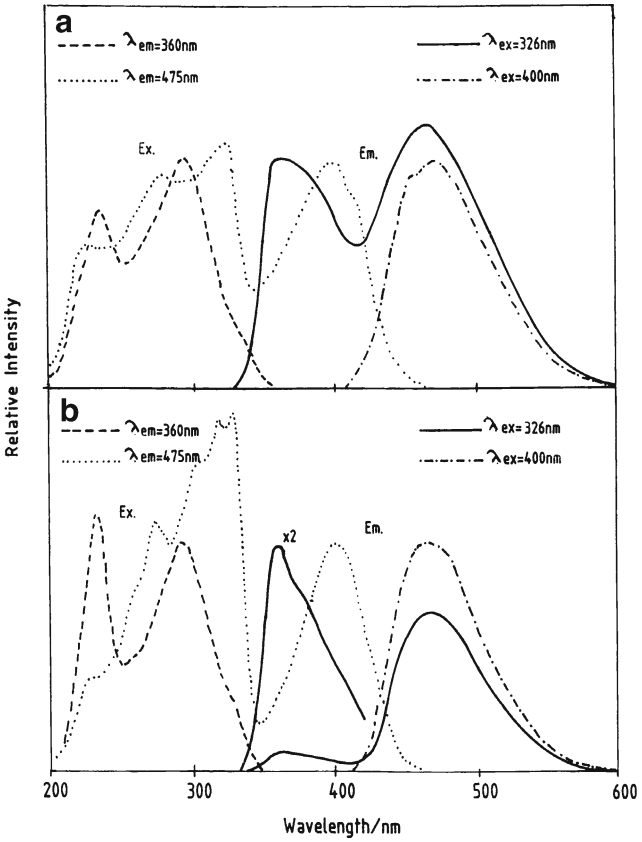

Fig. 4 Normalized emission and fluorescence excitation of compounds: **1** (**a**) and **2** (**b**) in *n*-hexane

Fluorescence spectra of compounds **1** and **2** (Fig. 4a-b) are dependent on the excitation wavelength. Thus excitation to the maxima of band **III,** produced dual emission bands consisting of a short-wavelength (SWE) slightly structured band around 350–400 nm, and a long-wavelength (LWE) broad band in the region 400–600 nm. However, excitation at wavelength corresponding to absorption maxima of band **IV**, gives exclusively the long wavelength emission broad band centered around ca. 475 nm. This emission originates from $S_0 \leftarrow S_1$, while the LWE is of S_2 origin (see Fig. 4a-b and Table 1).

The emission from the S_2 and S_1 states for compound **1** is of equal intensity, while the emission from $S_0 \leftarrow S_2$ in compound **2** is seen as a weak one.

Excitation spectra of compounds **1** and **2** in non-polar *n*-hexane, give a single band when monitored at wavelength of the short-wavelength emission band (SWE); but produced dual excitation bands when the emission tuned at the maxima of the long wavelength emission band (LWE) (see Fig. 5a-b).

The measured excitation spectra in non-polar solvents, monitored at both the high and low wavelengths emission bands matches with the corresponding absorption spectrum. Thus, we conclude that these molecules exists as a single species in the ground state; and the dual fluorescence emission is thus attributed to existence of two excited states species which are S_1 and S_2 states with the former possessing charge-transfer.

Emission Spectra in Polar Aprotic and Protic Solvents

Both compounds **1** and **2** exhibit solvent-dependent fluorescence emission spectra. Figures 5a-b, display emission spectra for compounds **1** and **2** in *n*-hexane, *n*-butanol and acetonitrile. It is evident that excitation of compounds **1** and **2** at the maxima of band **III** in polar low hydrogen-bonding solvents such as acetonitrile, gives rise to emission from the S_2 state ($S_0 \leftarrow S_2$) with a shoulder in the range 450–500 nm (LWE) and tailing to the red. However, only one broad band representing emission of the S_1 state ($S_0 \leftarrow S_1$) is given when

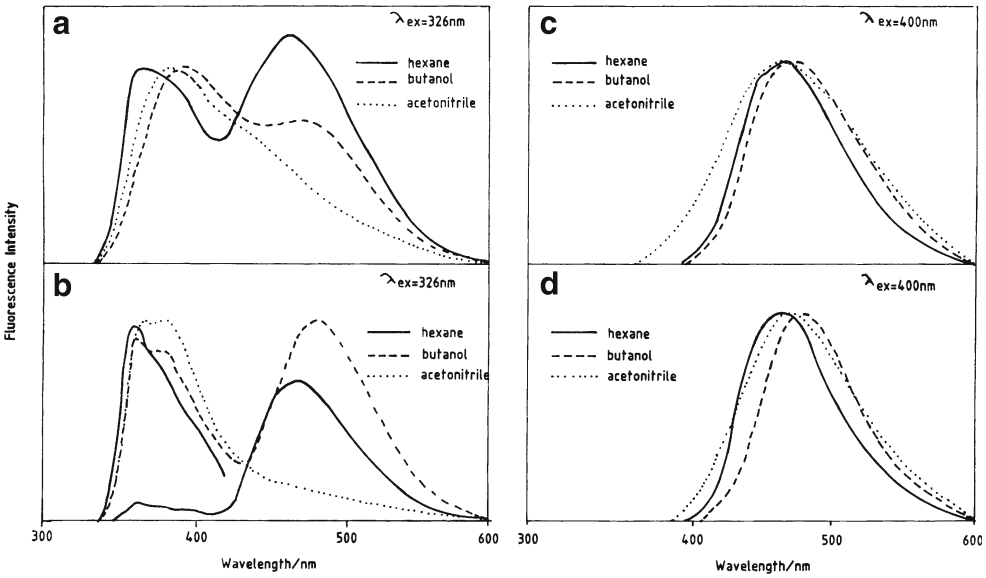

Fig. 5 Effects of excitation wavelength on fluorescence of compounds: **1** (**a** and **c**) and **2** (**b** and **d)** in a polar aprotic (acetonitrile) and polar protic (butanol) solvents. (**a)** and (**b**), λ_{exc} = 326 nm. (**c**) and (**d**), λ_{exc} = 400 nm. Spectra of *n*-hexane are included for comparison

these two compounds were pumped at the maxima of band **IV** ($S_1 \leftarrow S_0$, λ = 400 nm).

On the other hand, the situation is different in polar strong hydrogen bonding solvents such as hydroxylic solvents. Thus excitation of compounds **1** and **2** at the maxima of band **III** ($S_2 \leftarrow S_0$, λ = 326 nm) produce dual fluorescence originating from both S_1 and S_2 states. In compound **1**, the maxima of the S_2 emission is red-shifted by ca. 28 nm (0.24 eV) on going from *n*-hexane to *n*-butanol, compared to S_1 state, which shift only ca. 5 nm (0.05 eV). These results, suggest the relatively higher dipolar character of this state (S_2) compared to S_1 state. Compound **2**, on other hand, show solvatochromic shift of the S_2 state emission by only ca. 10 nm (0.1 eV). This is depicted in Fig. 5a-b, for fluorescence emission of compounds **1** and **2** in *n*-hexane, *n*-butanol and acetonitrile.

Our results also show that, when the excited wavelength is tuned at the peak of band **IV**, emission of the S_1 state is exclusively obtained regardless of the type of the solvent used (Fig. 5c-d). The solvatochromic shift of this state from *n*-hexane to acetonitrile is ca. 22 nm (0.19 eV) and 10 nm (0.1 eV) on going from *n*-hexane to acetonitrile for compounds **1** and **2**, respectively (see Figs. 5a-b).

In our systems (based on the measured exCitation spectra) we estimate an energy gap ($\Delta E_{S2\text{-}S1}$), ca. 5855.7 cm^{-1} and ca. 5444.4 cm^{-1} in *n*-hexane for compounds **1** and **2**, respectively. On the other hand; our DFT calculations (full discussion of which will follow) gives an energy separation of ca. 4146.6 cm^{-1} and 4332.9 cm^{-1} in the gas phase (4212 cm^{-1} and 4754 cm^{-1} in cyclohexane) for the same compounds, respectively (see Table 2)

Table 2 Selected structural parameters of the most stable structure of compounds 1–2 in the ground-state (S_0) calculated in the gas-phase at DFT/b3lyp/6–31 + G(d,p) level

Parameters	1 S_0	2
Bond lengths (A°)		
R(C1-C2)	1.41819	1.40016
R(C2-C3)	1.41355	1.41319
R(C3-N32)	1.33040	1.32934
R(C4-S32)	1.33673	1.34072
R(C4-C5)	1.42417	1.42103
R(C1-C5)	1.40391	1.39301
R(C2-C8)	1.45329	1.44542
R(C3-S7)	1.74847	1.75290
R(S7-C19)	1.77944	1.78766
R(C8-C19)	1.40352	1.40027
R(C19-C20)	1.45030	1.45113
R(C20-C14)	1.50181	1.50117
R(C9-C14)	1.40463	1.40475
R(C9-C10)	1.39372	1.39373
R(C10-C11)	1.39933	1.39932
R(C11-C12)	1.39656	1.39663
R(C12-C13)	1.39733	1.39726
R(C13-C14)	1.40336	1.40342
R(C20-O25)	1.24989	1.24880
R(C8-N21)	1.36369	1.35844
R(C1-C6)	1.51322	1.08874
R(C4-C27)	1.51105	1.51485
	1.51581 R(C5-C26)	1.51940 R(C1-H6)
Bond angles (°)		
A(C19,C8,N21)	122.1732	124.229
A(S7,C19,C20)	124.0811	124.767
A(C19,C20,O25)	120.6268	120.069
Torsion angles (°)		
D(C13,C14,C20,C19)	42.781	41.45
D(C9,C14,C20,O25)	37.855	36.949
D(C8,C19,C20,O25)	2.6699	3.31893

Theoretical Calculations

Potential-Energy Curves

We performed calculations of the potential energy as a function of the available relaxation channels, *i*) the phenyl and, *ii*) the benzoyl groups. The angles ϕ_1 = C8-C19-C20-O25 and ϕ_2 = C19-C20-C14-C9 were varied from 0° to 180°, with a grid size of 10°. The results of the potential energy profiles are given in Figs. 6 and 7. Our calculations at 6-31G+(d,p) gave a total of three stable conformers named hereon conformers **a,b** and **c** (Fig. 8). The global minima found at $\phi_1(\phi_2)$ 2.669°(37.855°) and 3.3189°(36.949°), which correspond to electronic energies of ca. 778,355.454 and ca. 802,270.14 Hartree for compounds **1–2**, respectively (Figure S1).

Twisting of the phenyl motif starting from the global minimum, gives rise to another iso-energetic conformer with different phenyl plane orientation. These minima are slightly higher in energy ca. 0.2429 and 0.1838 kcal mol^{-1} with respect to the global minima for compounds **1–2**, respectively.

It is found that the calculated energy differences, are much smaller than the thermal energy at 300 K (1.5kT ≈ 0.899 kcal mol^{-1}). Hence, it is expected that these structures coexist at room temperature and conversion between the two is a barrierless process.

On the other hand, twisting the benzoyl group starting from the global minima (conformer **a**) yield another minima higher in energy ca. 6.566 and 5.909 kcal mol^{-1}, for compounds **1–2**, respectively. In these higher energies, the carbonyl oxygen is in *syn* position to the sulfur and the pyridine-nitrogen atoms giving conformer **c** (Fig. 8). The calculated energy barrier for transformation of the *syn* position to the global minimum

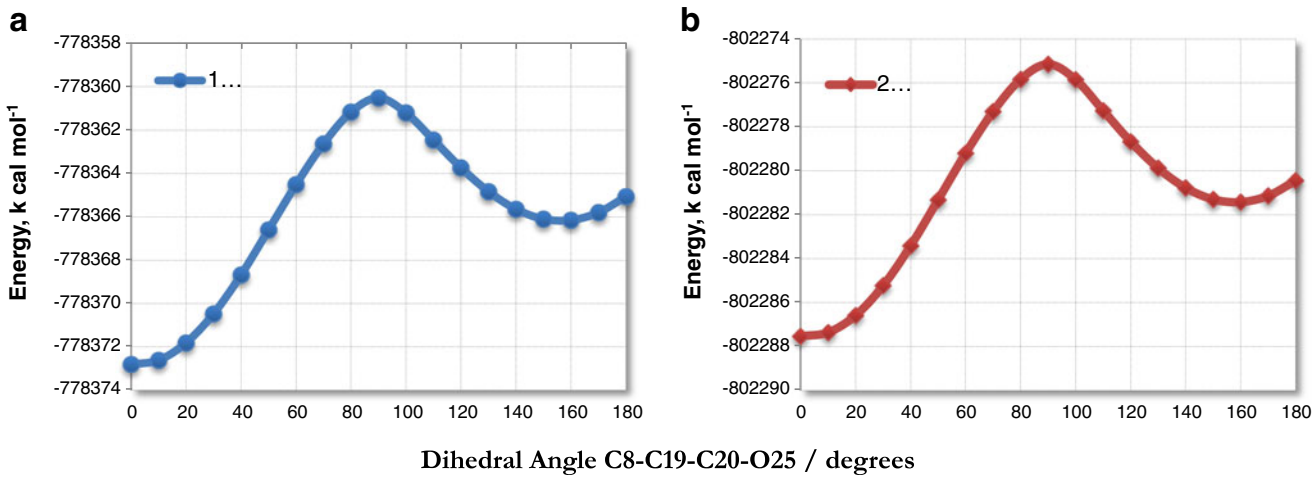

Fig. 6 Potential energy profile of the interconversion between conformers **a** and **c** of compounds: **1** (**a**, *blue*), **2** (**b**, *red*). The DFT/6–31 + G(d,p) calculations were done for the series of points of the dihedral where all degrees of freedom fully optimized

(*anti*) requires energies for compound **1–2** ca. 5.479 and 6.056 kcal mol^{-1}, respectively. The plane of the benzoyl motif in the *syn* structure (conformer **c**) is ca. 165° and 155° out of planarity with respect to the thiophene ring.

The most stable conformers (*anti*) of these compounds are characterized by the close proximity of the amine and the carbonyl groups, leading to a possibility of formation of intramolecular hydrogen bond (H-b). This H-b gives extra stabilization to these conformers in the S_0 state. Therefore, transformation from the most stable *anti* to the *syn* position evolves through large torsional barrier (ca. ΔE = 12.045 and ΔE = 11.966 kcal mol^{-1}, for compounds **1–2**, respectively). The closed ring formed in the *anti*-structure, gives the extra stabilization to the hydrogen bond NH…O structure. Indeed, our calculations for the stability gained (ca. ~ 12 kcal mol^{-1}) suggest occurrence of a strong hydrogen bond. The reported energy of an ordinary hydrogen bond in the literature is ca. 5 kcal mol^{-1} and in many cases it is ≥10 kcal mol^{-1} [39]. For instance, Deshmukh et al. estimated this H-b energy in polypeptides to lie in the range 4–6 kcal mol^{-1} [40]. Zhang Y. group studied the intramolecular of 10-membered ring NH…O hydrogen bond in glycine and alanine peptides and evaluated the binding energy to be 6.84–7.88 kcal mol^{-1}, using MP2/6–311++G(3df,2p) level of theory [41].

Based on the above findings, it is expected that conformer **a** (*anti*) will remain in this form due to the large energy required to populate the higher structure conformer **c**. Further, the large energy difference between conformer **c** (*syn*) and conformer **a** (*anti*) indicate that other factors beside the close proximity of the amine and the carbonyl groups, lead to a strong H-b.

To better understand the origin of the extra stabilization of the *anti* position, we carried out molecular electronic potential (MEP) on these compounds. Figure 9 gives the MEP surface of conformer **1a** and **1c** encoded onto total electronic density surface. It is evident that in conformer **1c** (where the oxygen is *syn* to the S and N atoms) the negative regions are very close creating great repulsion, which destabilize this structure.

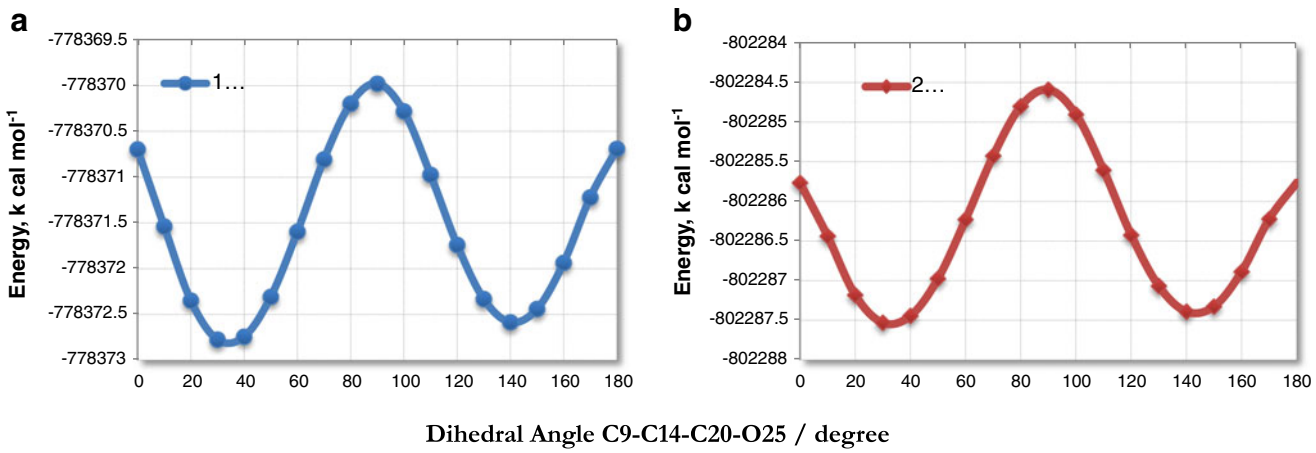

Fig. 7 Potential energy profile of the interconversion between conformers **a** and **b** of compounds: **1** (**a**, *blue*), **2** (**b**, *red*). The DFT/6–31 + G(d,p) calculations were done for the series of points of the dihedral where all degrees of freedom fully optimized

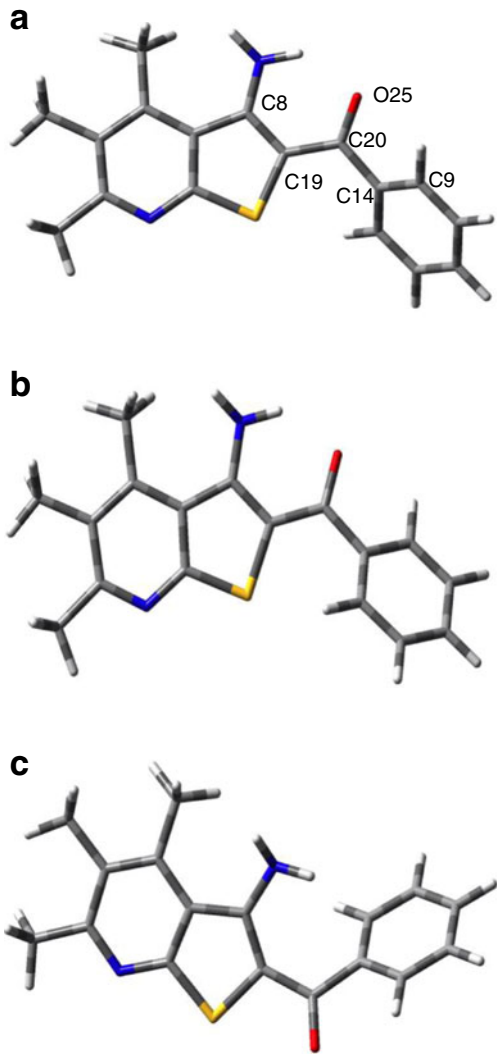

Fig. 8 Stable conformers: **1a**, **1b**, and **1c** of compound **1**. The major difference between the three conformers is the orientation of the phenyl ring (**1a** and **1b**) and orientation of the benzoyl group (**1c**). Atomic labeling for the dihedrals scanned as shown for structure **1a** is applied to all calculated in this study

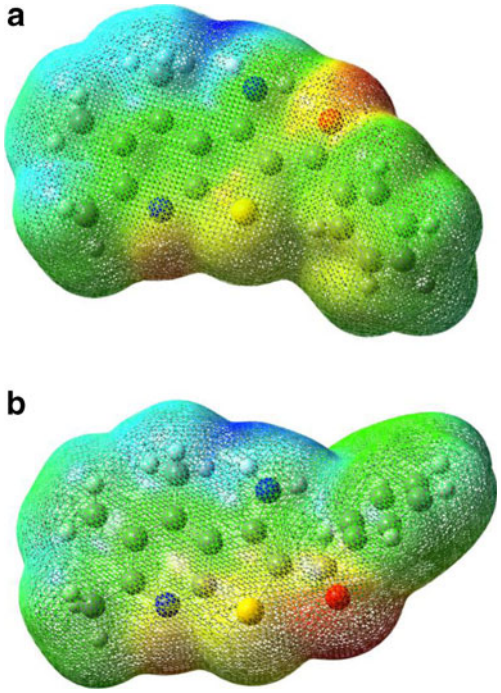

Fig. 9 Molecular electrostatic potential map of compound **1**: **a** lowest S_0 structure and **b** Twisted S_0 structure (second lowest) calculated at b3lyp/6-31G+(d,p) level. The electron density isosurface is 0.0004 a.u

However, in conformer **a**, the two most negative region are apart, and further, the negative region on oxygen is close to the most positive regions (around the amine-N). This charge accumulation stabilizes this structure by ca. 6.5663 kcal mol^{-1}. This situation is further enhanced by an intramolecular NH…O hydrogen bond, forming almost a planar 6-memebred ring (Table 2 and Fig. 3). The NH…O distances in these structures are ca. 1.865 and 1.925 A°, for compounds **1–2**, respectively. These short distances are within the reported intramolecular NH…O hydrogen bond [42].

Our DFT calculations show that the most stable gas-phase ground-state geometries of compounds **1–2** (Figure S1) have comparable dipole moments (~4D) implying weak charge transfer (ICT, discussion will follow) in the ground-state. In comparing the bond distances in compounds **1–2** as given in Figure S2, no remarkable differences were seen. However, some bonds in response to the solvent polarity as depicted in Figure S3, for compounds **1** (compound **2** not given), the carbonyl bond (C20-O25) elongates in the order gas-phase < CH < ACN ≈ EtOH. Also, the bond C8-C19 follows the same elongation with increasing solvent polarity. However, C19-C20 and C8-N21 bonds show contraction with increase in solvent's polarity (see Figure S3). It is observed that the lengthening of the carbonyl bond is accompanied by charge accumulation on the oxygen (=O25) and pyridine nitrogen (N32) atoms with increasing solvent polarity; and charge depletion from the carbon C20 and the carbon C1 (Figures S4 and S5).

In compound **1** for instance, the charge on oxygen increases from −0.497 (gas-phase) to −0.574 (EtOH) and decreases in C20 from +0.190 (gas-phase) to +0.367 (EtOH). Our results show that the amine-nitrogen is not the source of the charge delocalization since this atom does not show any response to the bulk solvent polarity. However, N21 shows sensitivity to solvent changes in compound **1** (Figures S4-S5 in the supporting information). The trend for the other equivalent atoms in compound **2,** are the same.

As a consequence to these changes of the simultaneous increase and decrease in negative charge along with C = O bond elongation, charge polarization is enhanced in polar solvents, leading to increase in intramolecular charge transfer (ICT). This ICT is further confirmed from the analysis of electron density on the highest occupied (HOMO) and the lowest unoccupied (LUMO) orbitals of these molecules that will follow.

Frontier Molecular Orbitals

In general, the plots of the HOMO and LUMO show typical π-type molecular orbital characteristic. The HOMO shows a bonding character and the LUMO represent an anti-bonding one. The HOMO is localized on the pyridine- and thiophene-rings, as well as, the amino-nitrogen and carbonyl-oxygen. Whereas, the lowest unoccupied molecular orbitals (LUMO); is delocalized on the whole molecule (Fig. 10, and Figures S6 in the supporting information). The lowest lying-singlet states are corresponding to electronic HOMO→LUMO transition (π→π* type, strong oscillator strength), while the second singlet state is populated by a combination of, HOMO-2➔LUMO (n_o→π*, weak oscillator strength) and HOMO-4→LUMO (π_{ph}→π*). Table 3 collects the assignments of some selected singlets and triplets transitions for compounds **1–2** in the gas-phase, while Fig. 10 and Figures S6 show the frontiers of the molecular orbitals (MO) involved in these transitions.

As observed in Table 3, Fig. 10 and Figures S6, the patterns of HOMOs and LUMOs of compounds **1–2** are qualitatively identical. Comparing the HOMOs and LUMOs energies of compounds **1–2**, we notice marginal changes, implying negligence impact of the fused alkyl group on them.

The TD-DFT calculations show that the lowest singlet state S_1 is drived exclusively by transition from the HOMO (involves the core pyridyl-thiophine ring) to the LUMO, which is delocalized on the whole molecule ($HOMO_{py\text{-}thio}$→LUMO). On the other hand, the second excited singlet state (S_2) is derived from HOMO-2 →LUMO transition and ($(HOMO\text{-}4)_{ph}$→LUMO). The MO of HOMO-4 is mainly centered on the phenyl ring. The adjacent triplet state T_2 is derived from HOMO-2, (58 %) and HOMO-1 (18 %) transitions for compound **1** and HOMO-2 (56 %) and HOMO-1 (27 %) in case of compound **2**. As seen in Table 3, the computed electronic transitions in the gas-phase nicely predict the measured ones in *n*-hexane.

Further inspection of Fig. 10 and Figures S6; show that there exist frontier orbital interaction (circled red in Fig. 10) between the C-H σ-orbitals of the substituents methyl/cyclic alkyl fused to the pyridine moiety at positions **1** and **2**, with the π-orbitals of these compounds. This σ-π interaction in the occupied MO is greater in the HOMO-1. Hence, methyl/alkyl substitution at this position enhances hyper-conjugation, and the fact that this MO is anti-bonding it is expected that this hyper-conjugation cause the HOMO-1 MO's of compound **1–2** to be destabilized.

Solvatochromism

Spectral Response to Various Solvent Scales

In order to evaluate the effect of solvent polarity and unravel which properties are the primary factors influencing the observed spectral changes, we carried out extensive analysis of the solvent dependence of the spectral shift using Kamlet-Taft hydrogen bond donor strength, (α) hydrogen acceptor strength (β) and the bipolarity/polarizability (π*) parameters [43]; in addition to the famous $E_T(30)$ empirical solvent introduced by Dimroth-Reichardt [44, 45].

We found that the plots of the absorption maxima of compounds **1–2** versus acidity constants (α) some selected polar aprotic and protic solvents, were scattered and no correlations were found (Figure S7). However, reasonable *r*-values obtained only for alcohols ca. 0.8987 and 0.8091 for compounds **1–2**, respectively. On the other hand, the plots of the absorption shift as a function of basicity (β) scale (Figure S8), gave reasonable correlation (r = 0.8700 and for compounds **1–2**, respectively.

Excellent fits were also found for the absorption in protic and aprotic solvents together as a function of solvent polarizability (π*). Indeed, the *r*-values found were 0.9005 for compound **1** and 0.9940 for **2** (see Figure S9). The fits of the absorption maxima versus π* gave better linear relationship in alcohols, as shown in Figure S10 (r = 0.9876 and 0.9997 for compounds **1–2**, respectively). On contrary, a linear relationship between υ_{abs} of compounds **1–2** versus the solvent

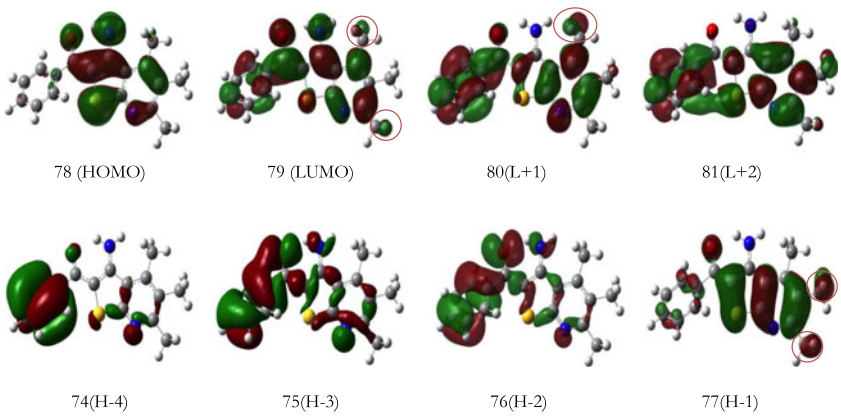

Fig. 10 Kohn-Sham frontier of the four lowest unoccupied and three highest occupied frontier molecular orbitals involved in the electronic transitions of compound **1** calculated in the gas-phase at the DFT/b3lyp/6–31 + G(d,p)

Table 3 Calculated electronic transitions energies, ΔE (in eV and nm), with oscillator strength, f, main assignment (configuration interaction coefficient) and Energy gap (ΔE_{gap}) for compounds 1–2 (conformer a) in the gas-phase, obtained from TD-DFT/b3lyp/6–31 + G(d,p) method

	1				2			
Transitions	ΔE			CI expansion coefficients	ΔE			CI expansion coefficients
	nm	eV	f		nm	eV	f	
S_0–S_1	390	3.18	0.1604	0.690 (HOMO → LUMO)	398	3.11	0.1296	0.690 (HOMO → LUMO)
S_0–S_2	336	3.69	0.0011	0.600 (HOMO-2 → LUMO) 0.031 (HOMO–4 → LUMO)	340	3.65	0.0025	0.580 (HOMO-2 → LUMO) 0.032 (HOMO–4 → LUMO)
S_0–S_3	313	3.96	0.0038	0.600 (HOMO → LUMO + 1) 0.310 (HOMO-1 → LUMO	317	3.90	0.0080	0.590(HOMO → LUMO + 1) 0.350 (HOMO-1 → LUMO)
S_0–T_1	577	2.15	0.0000	0.690 (HOMO → LUMO	581	3.12	0.0000	0.690 (HOMO → LUMO)
S_0–T_2	386	3.21	0.0000	0.580 (HOMO-2 → LUMO 0.810 (HOMO-1 → LUMO	390	3.18	0.0000	0.560 (HOMO-2 → LUMO) 0.270 (HOMO-1 → LUMO
S_0–T_3	368	3.36	0.0000	0.620 (HOMO-1 → LUMO) 0.230 (HOMO-2 → LUMO)	376	3.29	0.0000	0.620 (HOMO-1 → LUMO) 0.230 (HOMO-2 → LUMO)
S_0–T_4	359	3.45	0.0000	0.560 (HOMO → LUMO + 1)	362	3.42	0.0000	0.560 (HOMO → LUMO + 1)
ΔE_{gap}[a]	4146.60 [0.514]				43,329.0 [0.5372]			

[a] ΔE_{gap} is the energy gap in cm^{-1} [eV] between the S_1 and S_2 states

polarity parameter $E_T(30)$ was found only in alcohols (see Figure S11 [r = 0.9949 and 0.9610 for compounds **1–2**, respectively]).

Based on the above observations, it is evident that solvent polarizability effects in alcohols play the major role in the measured spectral shifts.

Further evidence that support this conclusion comes from the fact that position of υ_{abs} for compounds **1–2**, correlates excellently with $f(n^2) = (n^2 - 1)(2n^2 + 1)$ [r = 0.9892 and 0.9994 for compounds **1–2**, respectively (see Figure S12)]. Therefore, we conclude that explicit H-bonding interaction causes increase in polarization in these compounds since it is the main contributor to the solvent-dependent spectra properties of compounds **1–2**.

Intermolecular H-b Effects in Alcoholic Solvents

The interaction energy of a dimer is probably the most widely used and important criterion in justifying the presence of H-bond. Although it is difficult to properly evaluate the strength of an intramolecular H-bond, in contrast to intermolecular H-bond whose strength may be reasonably estimated through various approximated approaches [46–50].

Our findings have been substantiated by results of the theoretical modeling of compounds **1–2** with added one alcohol (methanol, ethanol. *n*-propanol and *n*-butanol) explicitly H-bonded to the oxygen atom of the carbonyl O = C group (see Figure S13 for compound **1-alc** complexes as an example).

We carried out optimization of this **1:1** complexes in the S_0 state in the gas-phase. Our calculations were carried out at b3lyp/6-31G+(d,p) level of theory on these complexes. From the calculated optimized structures of compounds **1** and **2**, alcohols and compounds **1**(**2**)**-alcohol** complexes; the interaction energies (ΔE_i) of these complexes are estimated by,

$$E_i = E_{\text{complex}} - E_{1(2)} - E_{alc} \quad (1)$$

Where, E_{complx} is the energy of compounds **1**(**2**) complexes, $E_{1(2)}$ is the energies of compounds **1** and **2** and E_{alc} is energy of the alcohol molecule in question. The energies of compound **1** and **2**, alcohols and the compound **1-alc** and compound **2-alc** complexes as well as the interaction energies (in kJ/mol); are summarized in Table 4. As shown in Table 4, the interaction energies (ΔE_i) are all negative, which indicates that hydrogen bonding indeed stabilizes the complexes.

It is documented in the literature based on the interaction energies, that hydrogen bonds are classified into weak (4.2–16.7 $kJmol^{-1}$), medium (16.7–63 kJ mol^{-1}) and strong (63–188 $kJmol^{-1}$) [51].

Our DFT calculations show that interaction energies in the gas phase, is in medium range [53.852 (54.932), 55.406 (56.820), 56.987(57.940) and 58.398 (60.699) kJ mol^{-1}, for

Table 4 Calculated energies (b3lyp/6-31G+(d,p) level) of compounds 1a (E_1) and 2a (E_2), alcohols (E_{alc}), complexes (E_{complx}) and interaction energies (ΔE_i); along with the Taft-Kamlet-Taft solvent scale parameters [a] and Dimroth-Reichardt empirical scale.[b]

	α	β	π*	$E_T(30)$	E_{complx} E_{alc}, E_1 E_2 (kJ/mol)	ΔE_i (kJ/mol)
Compound 1					3,256,788.060	
Compound 2					3,356,851.712	
Methanol	0.98	0.66	0.60	55.4	303,833.2719	
Ethanol	0.86	0.75	0.54	51.9	407,073.8228	
n-Propanol	0.84	0.90	0.52	50.9	501,299.2565	
n-Butanol	0.84	0.84	0.47	49.7	613,524.3767	
1-MeOH					3,560,675.184	53.852
1-EtOH					3,663,917.289	55.406
1-PrOH					3,767,144.304	56.987
1-ButOH					3,870,370.835	58.398
2-MeOH					3,660,739.916	54.932
2-EtOH					3,763,982.355	56.820
2-PrOH					3,867,209.364	57.940
2-ButOH					3,970,436.788	60.699

[a] Taft-Kamlet (α, β, and π*) solvent parameters taken from reference [52]

[b] Dimroth-Reichardt $E_T(30)$ kcal mol^{-1} empirical scale [53]

complexes of compounds **1(2)** with methanol, ethanol, *n*-propanol and *n*-butanol, respectively.

The measured absorption spectral shift for compound **1** from methanol to *n*-butanol (ca. 4.5 nm) is comparable to the measured for compound **2** (ca.4.5 nm). Whereas, the interaction energy difference from methanol to butanol for compound **1** is ca. 4.546 $kJmol^{-1}$ and for compound **2** is ca. 5.767 kJ mol^{-1}; which implies a much stronger association of the solute with the alcohols in case of compound **2** compared to compound **1**.

We then attempted to correlate the absorption shift of compounds **1–2** in alcohols versus the calculated interaction energies. Excellent correlations were found as shown in Figures S14 and S15**,** which give the measured absorption maxima for compounds **1** (r = 0.9413 and 0.89928 for compounds **1** and **2** complexes, respectively).

Based on the above results, we went a step further in our investigation in order to find the most crucial solvent polarity influencing the interaction energies. Hence, we attempted to correlate the calculated interaction energies with α, β and π* (Kamlet-Taft solvent properties). However, these plots for the complexes of compounds **1** and **2** gave poor fits for α and β. However π* and $E_T(30)$ gave adequate linear correlation (r = 0.9662, 0.9737(π*) [Figures S16 and S17] and 0.9134, 0.9134 ($E_T(30)$) [Figures S18 and S19] for compound **1-** and **2-alc** complexes, respectively.

These linear correlations with π* and $E_T(30)$ strongly suggest the presence of specific interactions discussed earlier.

Intermolecular H-b Effects in Mixed Solvents

It is well known that changing the composition of the solution mixture, will change i) the local polarity of the solvation shell surrounding the solute, ii) increase/decrease the specific intermolecular solvent-solvent interactions; e.g. hydrogen bonding (H-b).

In pure solvents, the composition of the local solvation shell surrounding the solute is the same as the bulk solvent. This situation is totally different in mixed solvents, where in the binary mixture; the solute interacts differently where it is expected that one of the solvent will solvate the solute better than the other by means of one or more of dipole-dipole, dipole-induced dipole or hydrogen bonding (H-b). These solute-solvent interactions [52], have significant effect on the electronic spectra of the solute; by changing the intensity, shape and U*V*/*vis* absorption or/and emission (fluorescence) band position of the solute [53]; mainly σ→σ*, *n*→σ*, π→π*, *n*→π* and charge transfer (CT). The later three transitions are of importance in the study of organic chromophores.

In order to gain more insight into the specific role of the bulk solvent and specific solvation on the spectral features of compounds **1–2**; we then investigated the effects of intermolecular H-b on the fluorescence of compound **1.** We used a mixture of ethanol (polar-protic) and acetonitrile (polar-aprotic) solvents as an example and measured the fluorescence at r.t. It is observed that the high intensity fluorescence in ethanol (EtOH) is quenched upon gradual addition of acetonitrile (ACN) (Figure S20), with gradual blue shift of the emission maxima and appearance of some vibrational features. This quenching follows the stern-Volmer relationships [54]

$$\frac{I_o}{I} = 1 + K_{SV}[Q] \tag{2}$$

Where, $\boldsymbol{I_o}$ and $\boldsymbol{I}$ represent the fluorescence intensities in the absence and presence of acetonitrile, $\mathbf{K_{SV}}$ is the **S-V** constant. The Stern-Volmer plot from the steady state fluorescence quenching data based on Equation 2, did not show a linearity dependence rather an up-ward curvature (see inset in Figure S20), which indicate that the quenching mechanism follows the static model [54]. In this case, the acetonitrile molecule is replacing the alcohol; which is in contact with the fluorescent molecule thus destabilizing it (blue-shift). Therefore, we conclude that the emitting state is better stabilized in alcohols through H-bonding. Although ethanol is less polar than acetonitrile [Ethanol (ε = 24.3) vs. acetonitrile (ε = 37.5)], it has the capacity to form intermolecular H-bond with these compounds induces the shift of the excited energy. Thus it is evident that polarity of the shear solvent is not the main contributor for this states relaxation. It is apparent that these compounds become better polarized in alcohols

through explicit H-bonding. Thus, the energy of the ICT fluorescence state; can be more easily lowered by H-bonding. Further, addition of the polar solvent e.g., acetonitrile enhances energy dissipation through internal conversion (IC) or intersystem crossing (ISC).

Vibrational Analysis

NH_2 and C = O Stretching and Scissoring Vibrations

To gain more information on the existence of hydrogen bonding in compounds **1–2**, we carried out theoretical vibrational analysis of different stable conformers found (see **section 4.1**), along with the complexes with one alcohol molecule (e.g., ethanol). As discussed earlier, in compounds **1–2** evidence was given for the existence of intramolecular H-bond, where the acidic hydrogen of the amine (H-N) and the carbonyl oxygen (C = O) are the sites of this H-b.

Since complex formation predominantly involves the N-H and the C = O bonds, it is expected that complexes formation through specific interactions affect the corresponding stretching vibrations, υ^{a}_{NH2} , υ^{S}_{NH2} and υ^{S}_{CO}. The calculated vibrational wavenumbers of these bands for conformer **1a** (the global minima), **1c** (the second stable structure) and the complexes of the alcohol molecule with conformer **1a** are summarized in Table 5; whereas, the simulated IR spectra are given in Figure S21.

Based on literature search, it is reported that the NH_2 symmetric vibrations give rise to a weak band in the region 3150–3270 cm^{-1}, whereas, the asymmetric stretching vibrations give-rise to a strong band in the region 3330–3450 cm^{-1}, and the bending vibrations of NH_2 is located in the region 1580–1640 cm^{-1} [55, 56].

We found that the asymmetric NH_2 vibration (υ^{a}_{NH2}) shifts to lower energy upon changing from structure **1a** to **1c** (ca. shift 69.6 cm^{-1}) and is blue-shifted (ca. 24 cm^{-1}) upon complexation with one ethanol molecule (Figure S21 and Table 5 and Fig. 10). On the other hand, the calculated change in the symmetric stretching vibrations (υ^{S}_{NH2}), is blue-shifted by 102.3 cm^{-1} going from conformer **1a** to **1c**, and by only 90.8 cm^{-1} in case of the complex. Surprisingly, the scissoring vibration (δ^{SC}_{NH2}) mode is shifted to higher energy from conformer **1a** to conformer **1c** (ca. shift by 40.0 cm^{-1}) and by only ca. 2.9 cm^{-1} upon complex formation. These results suggest

Table 5 Calculated vibrational frequencies (in cm^{-1}) and IR Intensities for conformers 1a, 1c and conformer 1a + EtOH (complex) in the gas-phase obtain from DFT/b3lyp/6-31G+(d,p)

Mode	Conformer 1a	Conformer 1c	Complx
υ^{a}_{NH2}	3721.6 (82.99)	3652.0 (43.46)	3745.6 (111.95)
υ^{S}_{NH2}	3448.3 (89.57)	3550.6 (28.71)	3539.1 (223.51)
δ^{SC}_{NH2}	1632.2 (385.95)	1672.2 (123.30)	1635.1 (337.37)
υ^{a}_{CO}	1657.2 (107.93)	1689.6 (214.73)	1644.8 (124.60)

Type of vibrations:υ^{a} - asymmetric stretching, υ^{s} - symmetric stretching, δ^{SC} - scissoring

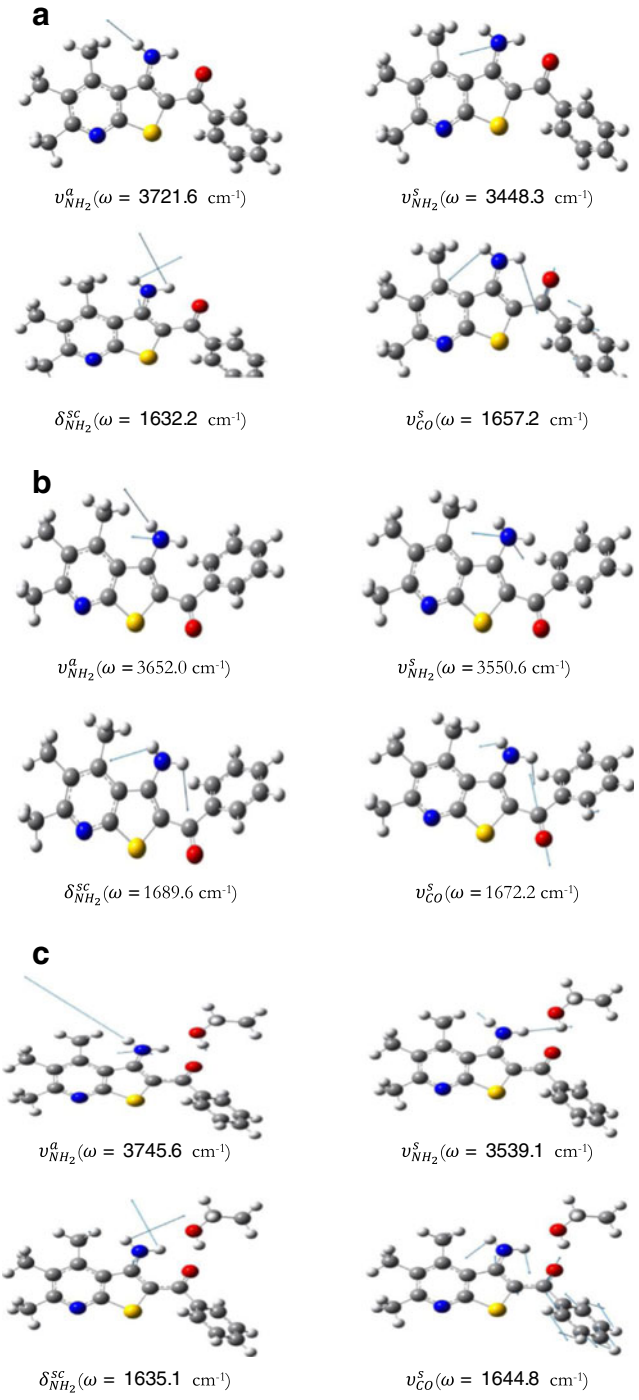

Fig. 11 Symmetric and asymmetric NH_2 stretching and NH_2 scissoring modes and C = O stretching modes of: **a** conformer **1a**, **b** conformer **1c** and **c** conformer **1a** + **EtOH** complex

that explicit addition of a single ethanol molecule marginally affect δ^{SC}_{NH2} compared to υ^{a}_{NH2} or υ^{S}_{NH2}, with the later motion being the mostly affected.

Therefore, the fact that the asymmetric υ^{a}_{NH2} and the symmetric υ^{S}_{NH2} stretching and the asymmetric scissoring modes (δ^{SC}_{NH2}) are blue-shifted compared to the bare molecule (conformer **1a**) implies that solvent molecule influence these vibrations in compounds **1–2**, in peak positions (to higher energy) and intensity (increase in stretching modes) as reported in Table 5.

The stretching wavenumber of hydrogen bond (H-b) acceptor (C = O) is red-shifted in the complex by ca. 12.4 cm^{-1} and ca. 44.8 cm^{-1} (elongation of C = O bond) with respect to the hydrogen bond free C = O conformer **1a**, and conformer **1c**, respectively. The shift in conformer **1c** is greater than **1a**, since the intramolecular H-b is broken in conformer **1c** and the carbonyl oxygen is exposed to intermolecular H-b. This explanation is supported by the MEP map calculated (see Fig. 9).

The calculated shifting difference of the stretching wavenumber between conformer **1c** and the global minima structure **1a** (ca. 32.4 cm^{-1}) suggest involvement of the N-H bond in intramolecular hydrogen bonding with the neighboring C = O group (H-b is absent in conformer **1c**). This is clearly reflected in the intensity of the C = O stretching vibration, where it is ~2 times more in conformer **1c** compared to **1a**.

The carbonyl C = O stretching (υ^{S}_{CO}) in the complex is red-shifted (ca. 44.8 cm^{-1}) with respect to the free conformer **1a**, as a consequence of weakening the C = O covalent bond (C = O involved in H-b). Whereas, the intensity of this mode does not change versus the un-complexed molecule **1a**, a manifestation of direct coupling to the vibrational degree of freedom of the solvent molecule as depicted in Fig. 11.

Conclusions

In this work, we have presented a combined experimental and computational study on two structurally related compounds with either tri-methyl substitution (**1**) or fused cyclohexyl (**2**) at the pyridinium ring. The electronic absorption, excitation and emission behavior of these compounds reveal that the excited-states S_1 and S_2, are populated directly in non-polar protic/aprotic solvents. These compounds showed excitation dependency and giving dual emission. In general, fluorescence of compounds **1–2** is enhanced in protic solvents, and the energy of the ICT fluorescence state is easily lowered by intermolecular hydrogen bonding.

Furthermore, the computational analysis on the present compounds shows that they exist in two structures: *anti* (conformer **a**) and *syn* (conformer **c**) with the later being lower in energy by ca. 5–6 kcal mol^{-1}. Transformation of the *syn* to *anti*-structure requires an energy ~12 kcal mol^{-1}. The *anti*-structure is stabilized through intramolecular NH…O hydrogen bonding (H-b).

Evidence was given that methyl/alkyl substitution in the pyridyl-thiophene ring, involve in σ-π hyper-conjugation and this leads to destabilization of the HOMO-1 MO's.

References

1. Dabkowska I, Gonzales HV, Jurecˇka P, Hobza P (2005) J. Phys. Chem. A 109:1131–1136
2. Zhao G-J, Han K-L (2012) Acc Chem Res 45:404–413
3. Zhao G-J, Han K-L, Stang PJ (2009) J Chem Theory Comput 5: 1955–1958
4. Zhao J, Ji S, Chen Y, Guo H, Yang P (2012) Phys Chem Chem Phys 14:8803–8817
5. Arunan E, Desiraju GR, Klein RA, Sadlej J, Scheiner S, Alkorta I, Clary DC, Crabtree RH, Dannenberg JJ, Hobza P, Kjaergaard HG, Legon AC, Mennucci B, Nesbitt DJ (2011) Pure Appl Chem 83(8): 1637–1641
6. Bruni P, Conti C, Galeazzi R, Giardina A, Giorgini E, Maurelli E, Tosi G (1999) J Mol Struct 480–481:379
7. Tekin N, Namli H, Turhan O (2005) Vib Spectrosc 39:214
8. Sun JQ, Xua L, Tang YQ, Chen FM, Liu WQ, Wu XL (2011) J Hazard Mater 191:62
9. Tekin N, Pir H, Sagdinc S (2012) Spectrochim Acta A Mol Biomol Spectrosc 98:122
10. Luzar A, Chandler D (1996) Phys Rev Lett 76:928–931
11. DeChancie J, Houk KN (2007) J Am Chem Soc 129:5419–5429
12. Zhang M-X, Zhao G-J (2012) Chem Sus Chem 5:879–887
13. V. Srinivasadesikan, P. K. Sahu, S-L. Lee., Spectrochim Acta A Mol Biomol Spectrosc 120 (2014) 542–547
14. Polat T (2014) J Mol Struct 1067:261–270
15. Vaquero V, Sanz ME, Peña I, Mata S, Cabezas C, López JC, Alonso JL (2014) J Phys Chem A 118(14):2584–2590
16. Chudoba E, Nibbering T (1998) Elsaesser. Phys Rev Lett 81:3010–3013
17. Zhao GJ, Han K-L (2007) J Phys Chem A 111:9218–9223
18. G. J. Zhao and Ke-Li Han, J Phys Chem. *A* (2009), 113, 14329–14335
19. S. L. Grabowski, S. J.; Krygowski, T. M. Chem Rev (2005), 105, 3513–3560.
20. Procházková E, Čechová L, Janeba Z, DraČínský M (2003) J Organomet Chem 78(20):10121–10133
21. Jalbout AF, Ali Naseri M, Fazli M, Raissi H, Rezaei MK, Nowroozi A, De Leon A (2009) Int J Quantum Chem 109:1481–1496
22. Tayyari SF, Raissi H, Milani-Nehad F, Butler IS (2001) Vib Spectrosc 26:187–199
23. Wojtulewski S, Grabowski SJ (2003) Chem Phys Lett 378:388–394
24. Wojtulewski S, Grabowski SJ (2003) THEOCHEM J Mol Struct 621:285–291
25. Becke AD (1993) J Chem Phys 98:5648–5652
26. Lee C, Yang W, Parr RG (1998) Phys Rev B 37:785–789
27. Musin RN, Mariam YH (2006) J Phys Org Chem 19:425–444
28. Lenain P, Mandado M, Mosquera RA, Bultinck P (2009) J Phys Chem A 112:10689–10696
29. Gromak VV (2005) J Mol Struct Theochem 726:213–224
30. Deshmukh MM, Bartolotti LJ, Gadre SR (2008) J Phys Chem A 112:312–321
31. Nowroozi A, Raissi H, Hajiabadi H, Tahani PM (2011) Int J Quantum Chem 111:3040–3047

32. Rozas I (2007) Phys Chem Chem Phys 9:2782–2790
33. Gaussian 09, Revision B.01. M. J. Frisch, *et al*. Gaussian Inc., Wallingford, CT, U.S.A.
34. Casida, M. E. *Recent Advances in Density Functional Methods*; World Scientific, Singapore (1995).
35. Becke AD (1993) J Chem Phys 98:5648
36. C. Lee, W. Yang and R. G. Parr., Phys Rev, B37, 785 (1988).
37. Ditchfield R, Hehre W, Pople J (1971) Self-Consistant molecular-orbital methods. IX. An extended gaussian type basis for molecular orbital studies of organic molecules. J Chem Phys 54:724–728
38. V. Barone, M. Cossi, Quantum calculation of molecular energies and energy gradients in solution by a conductor solvent model. J Phys Chem, A 102 (1998) 1995–2001
39. A. Demeter, T. Bereces and K. A. Zachariasse, *J. Phys. Chem. A*. (2005), 109, 4611.
40. C. L. Perrin and J. B. Nielson, *Annual Review of Physical Chemistry.* Vol. 48:511–544 (19987)
41. M. M. Deshmukh and Gadres, R; *J. Phys. Chem. A*. (2009) July, 9, 113 (27): 7927–32.
42. Y. Zhang and C. S. Wang, *J. Comput. Chem*. (2009) June; 30 (8): 1251–60.
43. Emsley J (1980) Very strong hydrogen bonds. Chem Soc Rev 9(1): 91–124
44. M. J. Kamlet, R. W Taft, *J. Am. Chem. Soc.* (1976) 98, 377–383.
45. TM Krygowski, E Milczarek, P. K Wrona,. *J. Chem Soc. Perkin.* Trans 2 (1980), 563–1568.
46. Reichardt C, Welton T (2010) Solvents and Solvents Effects in Organic Chemistry, 4th edn. Wiley-VCH, Weinheim, Germany
47. Reichardt C (1994) Chem. Rev. 94:2319–2358
48. S. G. Estacio, P. Cabral do Couto, B. J. Costa Cbral, M. E. Minasda Piedade, J. A. Martinho Simoes. *J. Phys. Chem. A* (2004) 108, 10834.
49. Lipkowskia P, Kolla A, Karpfenb A, Wolschannb P (2002) Chem Phys Lett 360:256
50. Woodford JN (2007) J Phys Chem A 111:8519
51. Wendler K, Thar J, Zahn S, Kirchner B (2010) J Phys Chem A 114: 9529
52. G. A. Jeffrey, *Introduction to hydrogen bonding*. Oxford University Press, N Y (1989).
53. Suppan P, Ghoneim N (1997) Solvatochromism. The Royal Society of Chemistry, Cambridge, U.K.
54. Rao VNR, Singh S, Senthilanthan VP (1976) Chem Soc Rev 5:297
55. J. R Lakowicz, *Principles of fluorescence spectroscopy* , 3rd ed.; Plenum Press: New York (2006).
56. R. M. Silverstein; G. C. Bessler, *Spectrometric identification of organic compounds*, 2nd ed.; John Wiley and Sons. Inc., New York, (1967).